Electronic Supplementary Information for

A zinc-iron redox-flow battery under $100 per kW h of system capital cost

Ke Gong[1], Xiaoya Ma[1], Kameron M. Conforti[2], Kevin J. Kuttler[1], Jonathan B. Grunewald[1], Kelsey L. Yeager[1], Martin Z. Bazant[2,3], Shuang Gu[1], and Yushan Yan[1]**

[1]Department of Chemical and Biomolecular Engineering, University of Delaware, Newark, Delaware 19716, USA
[2]Department of Chemical Engineering, Massachusetts Institute of Technology, Cambridge, Massachusetts 02139, USA
[3]Department of Mathematics, Massachusetts Institute of Technology, Cambridge, Massachusetts 02139, USA
Correspondence and requests for materials should be addressed to S. G. (shgu@udel.edu), or Y. Y (yanys@udel.edu)

1. Experimental Methods

RFB assembly. The experimental setup of the Zn-Fe RFB consists of three blocks of electrolyte frames, two current collectors, two types of electrodes, two pieces of membranes, and necessary cell accessories such as gaskets, tubes, and pumps (**Fig. S7**). Electrolyte frames consist of solid PTFE blocks. The thickness of the recess area on the middle-electrolyte frame is 2.5 mm. Graphite blocks were used as current collectors. Gold-plated copper sheets were used as conductors to connect with battery test station. One piece of carbon felt (Alfa Aesar, 3.1 mm uncompressed) and two pieces of copper mesh (TWP, Inc., 30×30 grid per square inch, 0.5 mm thickness each) were used as the positive and negative electrodes, respectively. Either Nafion® 212 or 211 (Ion power, 50 and 25 μm respectively) was used as the cation-exchange membrane. Either FAA-3 (FuMA-Tech GmbH, 45 μm) or A901 (Tokuyama Co., 10 μm) was used as the anion-exchange membrane. All membranes were soaked separately in 3 M NaCl solution for 24 hours and thoroughly washed with DI water to remove residual surface NaCl before use. Both Viton® rubber (0.75 mm per piece) and PTFE-coated fiber (0.15 mm per piece) were used as gaskets. Viton rubber was used to contact with graphite block. PTFE-coated fiber was used to contact with middle electrolyte frame. Eight bolts were torqued to 16 lb ft to tighten the cell and provide firm compression between the electrode and the current collector. The electrolyte was actuated by a peristaltic pump (Cole Parmer, Masterflex® L/S 600 rpm) through PTFE-lined rubber tubes (Cole Parmer, ChemDurance® #16).

The Zn-Fe RFB was then connected and tested by a commercial battery test station (Arbin, BT2000). All battery test experiments were conducted at room temperature.

Measurements of cell resistance and electrode overpotential. Solutions of 1 M $FeCl_2$ in 1 M HCl, 3 M NaCl, and 0.5 M $Na_2[Zn(OH)_4]$ in 4 M NaOH were used as the initial positive, middle, and negative electrolytes, respectively. The battery was charged to 50% SOC prior to measurements of cell resistance and electrode overpotential. The middle electrolyte concentration was 2.5 M at 50% SOC. Nafion® 212 and FAA-3 were used as the CEM and AEM, respectively, in cell resistance studies. An Ag/AgCl reference electrode was immersed into positive (or negative) electrolyte to measure the positive (or negative) electrode potential; the electrode overpotential for a given current density was obtained by comparing the charge/discharge potential with open circuit potential. The cell resistance was obtained by dividing the potential difference between the two Ag/AgCl reference electrodes (one in negative electrolyte and the other in positive electrolyte) by the applied charge/discharge cell current. Conditions sampled were flow rates of 0−400 mL/min and current densities of 10−200 mA/cm^2. Resistances measured in the charging process were used for data analysis.

Polarization test. The polarization of the Zn-Fe RFB cell was tested with the same initial electrolyte compositions but at 70% SOC. A Nafion® 211 membrane and an A901 membrane were used as CEM and AEM, respectively. A plastic mesh (~3×3 grids per square inch, 0.5 mm thickness) was put into the middle-electrolyte frame to separate the two membranes, to maintain the middle-electrolyte gap at 0.5 mm, and to generate turbulence for improved mass transport. Alternating charge and discharge current was applied and cell voltage at each current density recorded. A flow rate of 150 ml/min was used during the tests.

Cycle test. The cycle test of Zn-Fe RFB cell was performed with the following electrolyte compositions: 0.6 M $FeCl_2$ and 0.5 M NaCl in 1 M HCl as the positive electrolyte, 3 M NaCl as the middle electrolyte, and 0.3 M $Na_2[Zn(OH)_4]$ and 0.5 M NaCl in 2.4 M NaOH as the negative electrolyte. A volume of 20 mL was used for all electrolytes. Addition of NaCl to the positive and negative electrolytes minimizes the water transport during the cycle testing. Nafion® 212 and FAA-3 were used as the CEM and AEM, respectively, for cycle testing. The first cycle was carried out by charging to a capacity of 240 mAh to maintain an SOC swing of 75%. The ending voltage of the first charge cycle was set as the cut-off voltage for the following 19 cycles: charge and discharge cut-off voltages were 2.3 V and 0.8 V, respectively. During testing, all electrolyte containers were sealed. A flow rate of 100 mL/min was used during the test.

Cost model. The RFB is priced analogously to published methods[1-3]. In the expression for effective voltage of a single cell (Eq. 2), activation overpotential is calculated from the Butler-Volmer equation and internal resistance from the Nernst-Einstein relation. The modeled results are

validated against experimental data (**Fig. S8**). Shunt current losses and pumping losses are added when describing the voltage for the whole system.

For every stack size, then, optimal performance is attained at the flow rate that minimizes the sum of overpotential during each flow-through and pumping loss from the pressure drop due to flow. Using the smallest necessary stack size at its optimal flow rate will in turn minimize capital cost. The stack is sized to meet fixed power and energy ratings (here, 1 MW and 8 MWh), at each current density within the practical range (*e.g.*, 10−200 mA/cm^2). The tanks are sized to meet the electrolyte needs of constant-power discharge (**Fig. S9**). Pricing information is referenced in detail in the **Supplementary Tables**.

2. Supplementary Figures

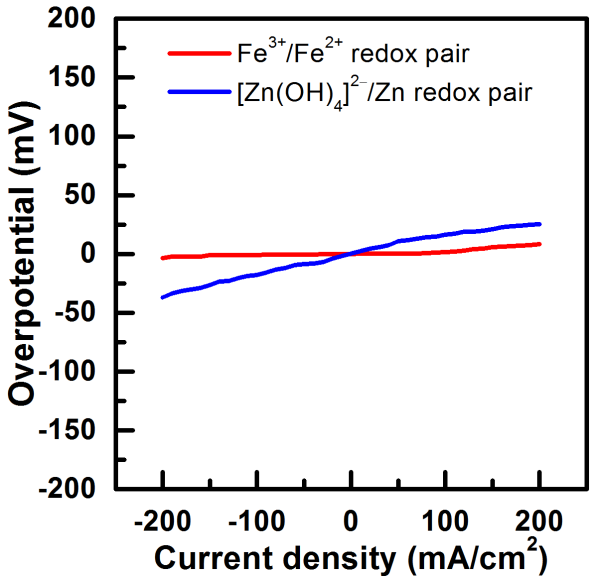

Figure S1 | Overpotential measured from zinc electrode (copper mesh) and iron electrode (carbon felt). The charge/discharge electrode overpotential is smaller than 10 mV and 40 mV for Fe^{3+}/Fe^{2+} redox pair (carbon felt electrode) and $Zn(OH)_4^{2-}/Zn$ redox pair (copper mesh electrode), respectively, at a current density of 200 mA/cm^2.Overpotential was measured in cell at 50% SOC.

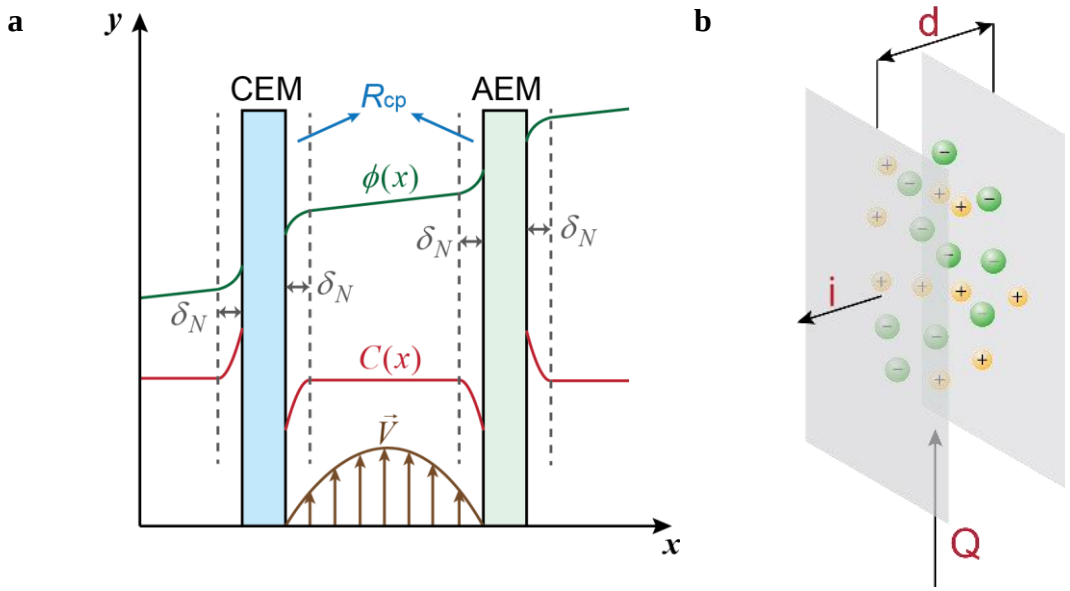

Figure S2 | Schematics of middle electrolyte in between two membranes (a) Schematic illustrating velocity, concentration, and potential profiles of middle electrolytes during charging process. Φ, C, V and δ_N represent potential, concentration, velocity and Nernstian boundary layer of electrolyte. **(b)** Schematic illustrating middle electrolyte and three key parameters (thickness, current density and flow rate) that influence the cell resistance.

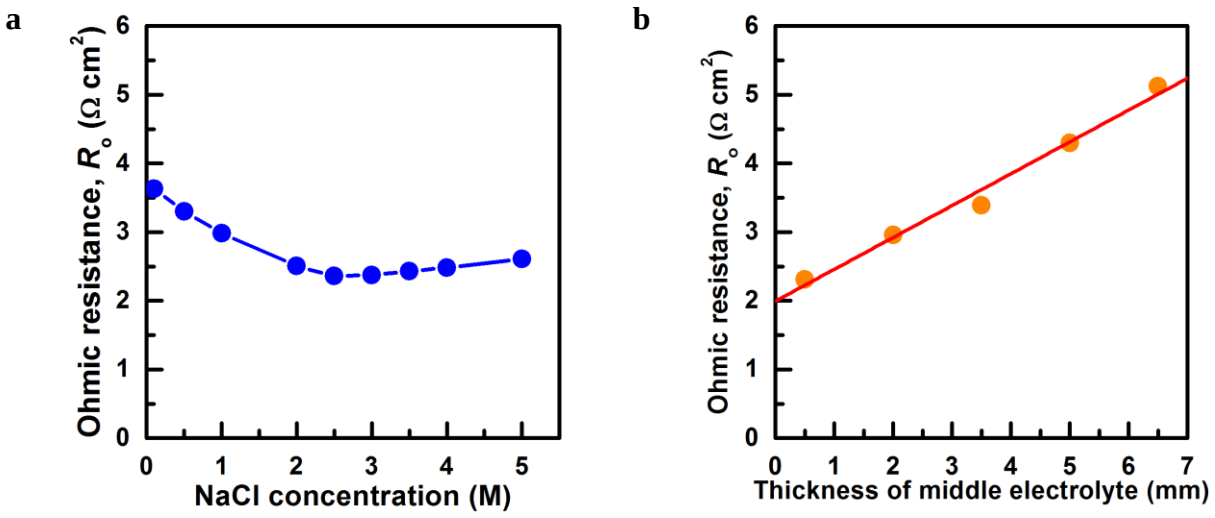

Figure S3 | The impact of middle electrolyte (thickness and salt concentration) on ohmic resistance. **(a)** The NaCl concentration vs. ohmic resistance at a middle electrolyte thickness of 0.5 mm. The ohmic resistance firstly decreases with raising NaCl concentration (increasing ionic conductivity of middle electrolyte), and after reaching the minima around 2.5 mol/L it slowly increases with raising NaCl concentration (decreasing ionic conductivity of membranes). The water content in membrane decreases when in contact with highly concentrated salt solution, resulting in lowered ionic conductivity. **(b)** The thickness of middle electrolyte vs. ohmic resistance at a middle electrolyte NaCl concentration of 2.5 mol/L. Note: in both cases, a low current density of 10 mA/cm^2 and a high flow rate of 400 ml/min were used to minimize concentration polarization.

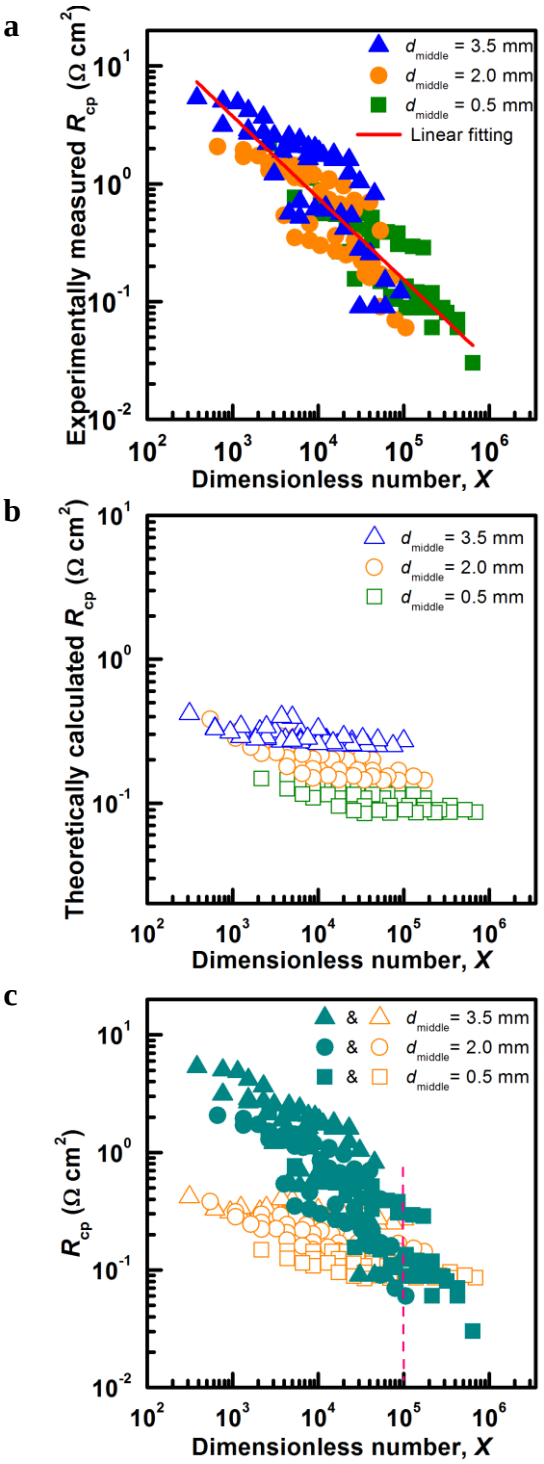

Figure S4 | Experimentally measured and theoretically calculated R_{cp} as a function of dimensionless number X. (a) Experimentally measured R_{cp} as a function of dimensionless number X and linear fitting on log-log scale. Linear fitting of log X vs. log R_{cp} shows a slope of −0.7, *i,e.*, as $R_{cp} \propto X^{-0.7}$. **(b)** Theoretically calculated R_{cp} as a function of dimensionless number X. We

calculated R_{cp} considering contributions from 1) the potential difference through the Nernst boundary layer in electrolyte adjacent to ion-exchange membrane and 2) the potential difference from the Donnan equilibrium across ion-exchange membranes (detailed in **Calculation Method**). **(c)** Comparison between theoretically calculated R_{cp} (empty symbols) and experimentally measured R_{cp} (filled symbols) with respect with the dimensionless number X. Both measured and calculated R_{cp} data have similar trend with respect with the dimensionless number X. It should be noted that the scaling law only roughly captures the trend of R_{cp} with X in both experiment and theory. The discrepancy at small X between experimentally measured and theoretically calculated R_{cp} is possibly due to the pressure differences between the middle electrolyte and the other two electrolytes. This pressure difference may cause the shape of the membranes to change from being flat to bent, consequently causing uneven flow distribution and extra R_{cp}. The theoretically calculated R_{cp} does not capture this effect and only illustrates the ideal scenario.

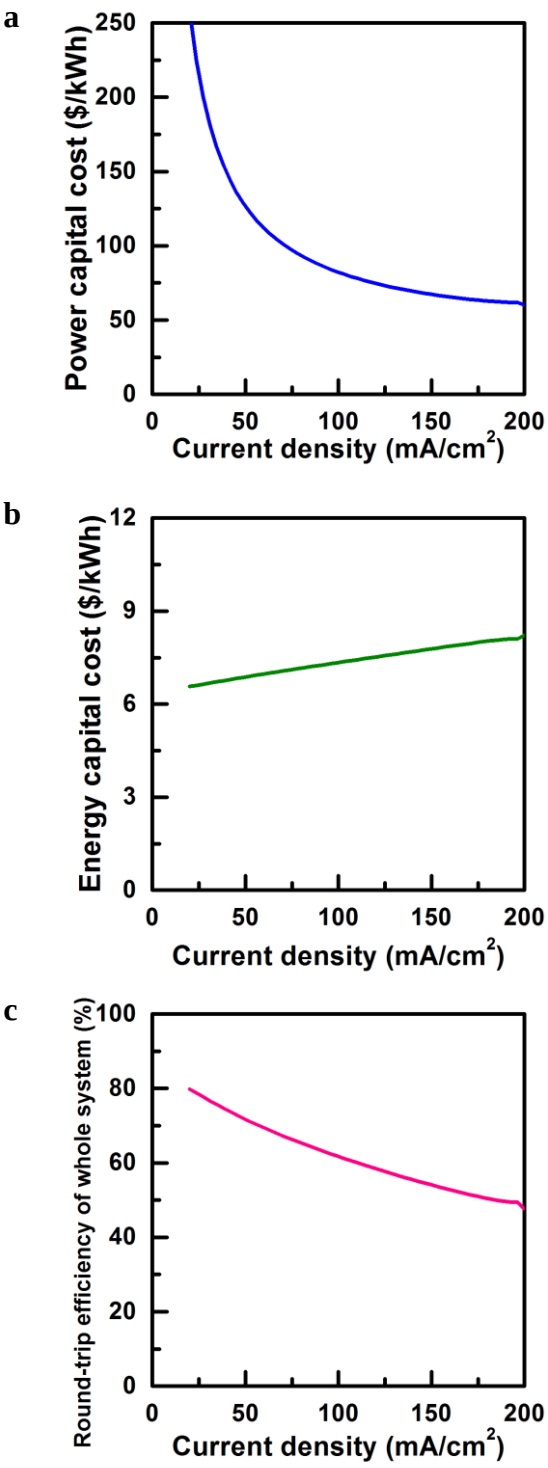

Figure S5 | Capital cost and round-trip efficiency of the whole system. (a) Power capital cost (mostly from stack cost). **(b)** Energy capital cost (mostly from electrolyte cost). **(c)** Round-trip efficiency of the whole system.

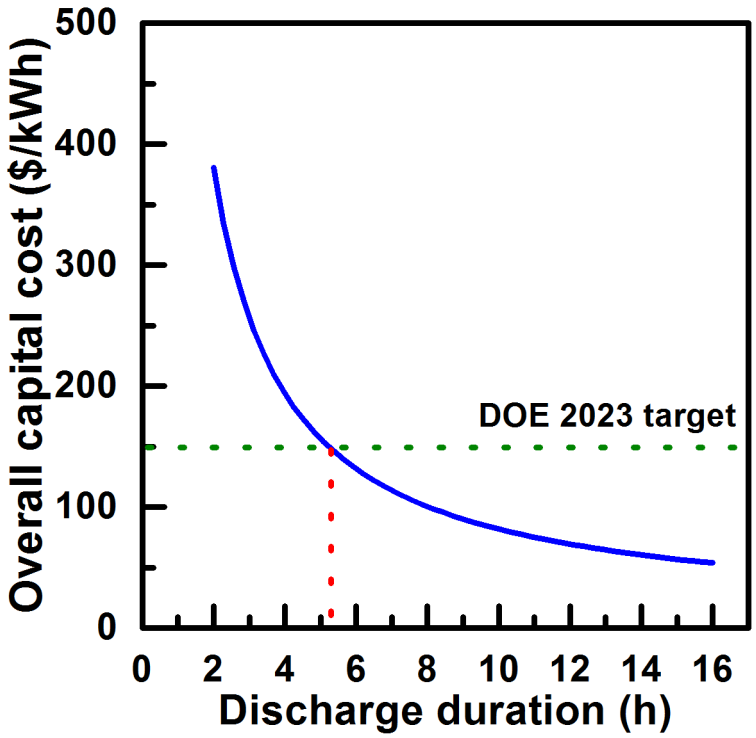

Figure S6 | System capital cost of a 1 MW Zn-Fe RFB system as a function of dishcarge duration at a curent density of 80 mA/cm^2.

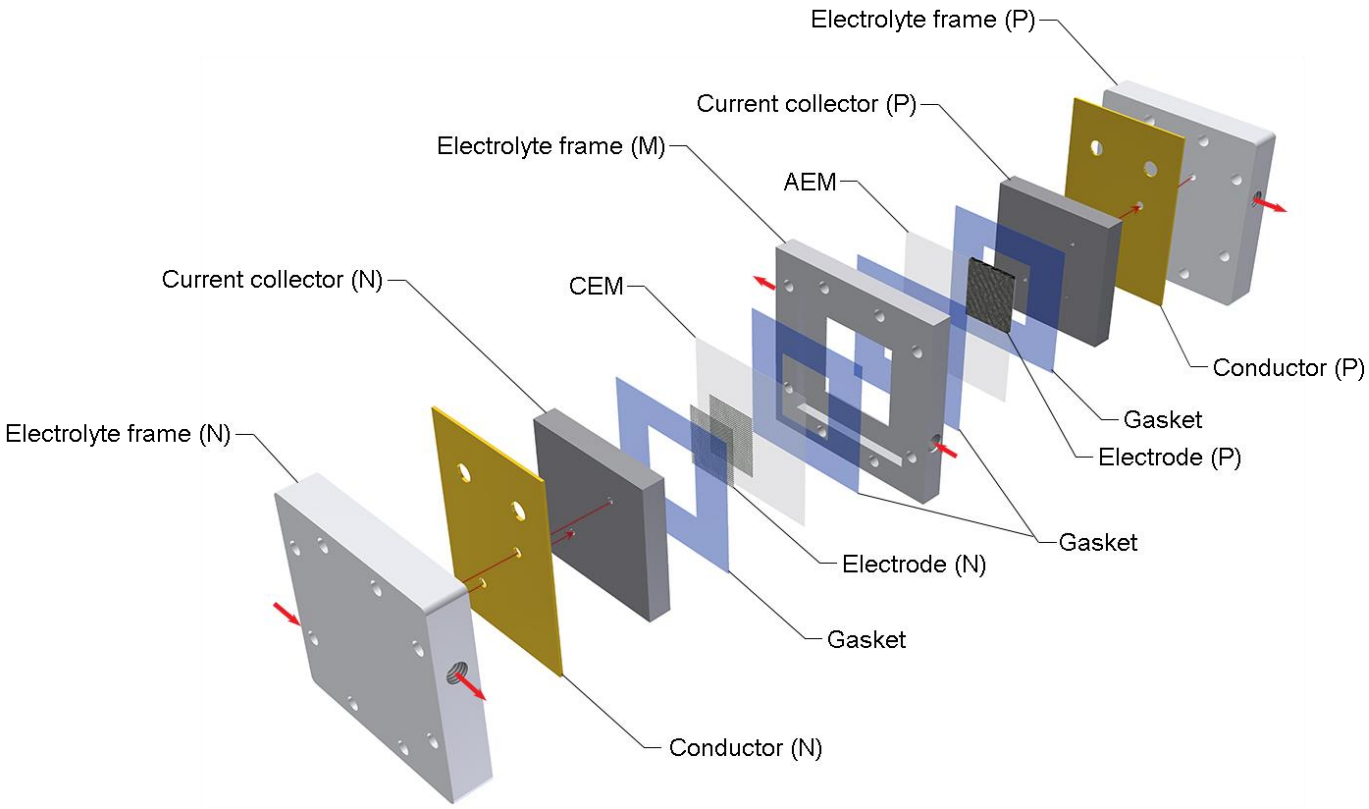

Figure S7 | Cell configuration of Zn-Fe RFB. The electrolyte flow pathways are shown with red arrows. The electrolytes enter and exit the system through the side holes on the electrolyte frames (thick red arrows). Once into the electrolyte frames, the positive and negative electrolytes flow sideway and through the small holes on electrolyte frame, conductor, and current collector into the chamber encompassed by gasket and membrane and then retrun to the electrolyte frames (thin red arrows). The middle electrolyte enters the middle electrolyte frame and then through the tiny hole on recesed portion of the middle electrolyte frame (not shown in figure) into the open area in middle electrolyte chamber defined by the two membranes. N, M, and P in parentheses stand for negative, middle, and positive, respectively.

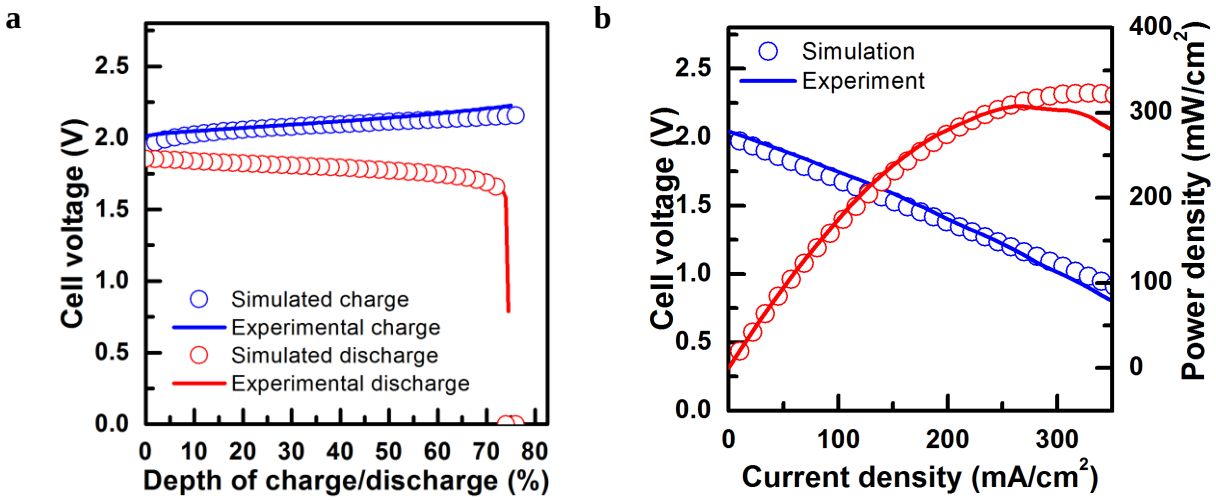

Figure S8 | Validation of electrochemical model for Zn-Fe RFB. (a) Charge and discharge curves at current density of 50 mA/cm^2. **(b)** Polarization and power curves at a SOC of 50%. Note: the polarization curve was obtained by using Nafion 212 and FAA membranes which have larger resistances compared with Nafion 211 and Tokuyama A901.

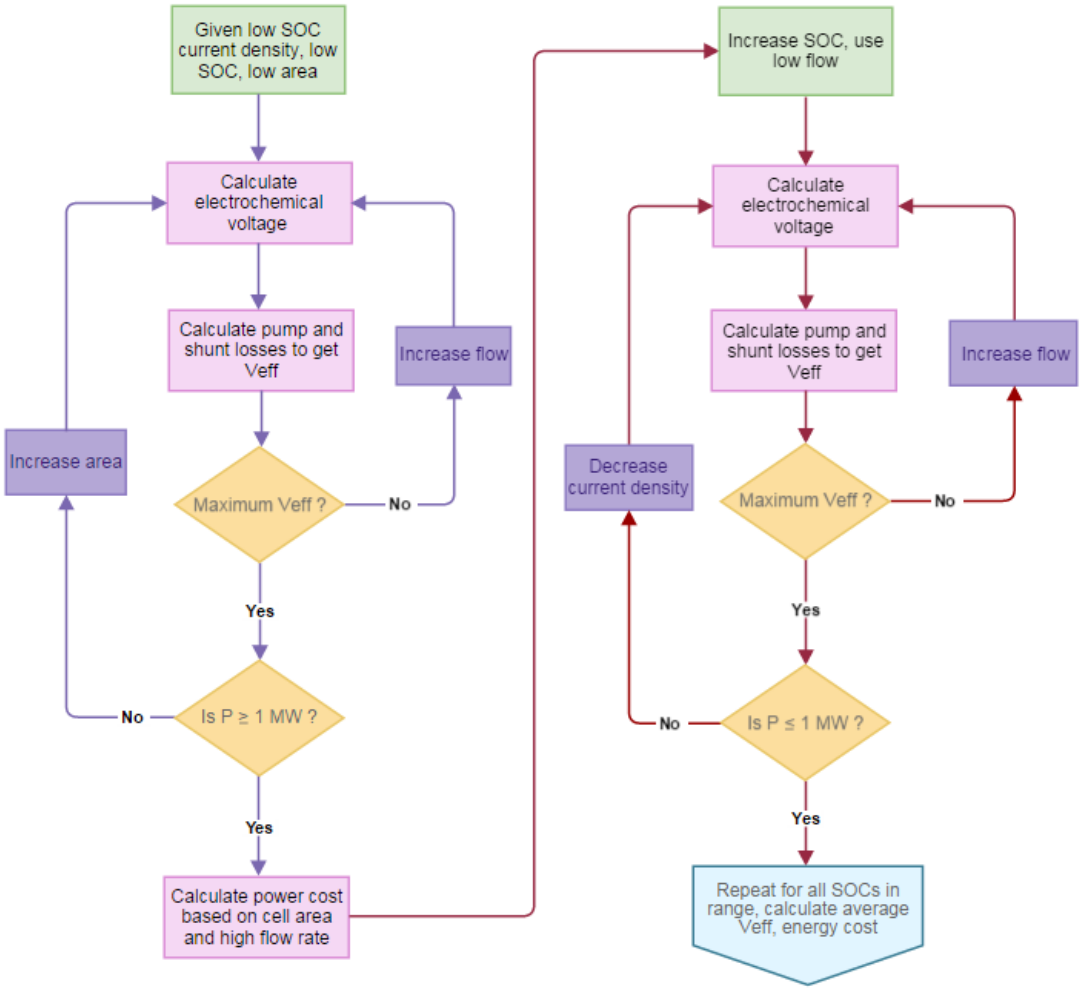

Figure S9 | Flow chart of simulation model algorithm. Reprinted from the reference 29 (*J Power Sources* **247**, 1040-1051) with permission from Elsevier.

3. Calculation Methods

3.1 Theoretical calculation of R_{cp}

Assuming electrolyte electroneutrality stands, R_{cp} can be calculated by the following equation:

$$R_{cp} = (\Delta\Psi_N + \Delta\Psi_D)/I \quad \text{Eq. 1}$$

where, $\Delta\Psi_N$ is the sum of all potential differences established through each Nernst boundary layer in the electrolyte adjacent to an ion-exchange membrane; and $\Delta\Psi_D$ is the sum of all Donnan potential differences built across each ion-exchange membrane between two different electrolytes; and I is current density.

Specifically, there are four Nernst boundary layers in the double-membrane cell: 1) in negative electrolyte adjacent to the CEM ($\Delta\psi_{n\text{-}c}$), 2) in middle electrolyte adjacent to the CEM ($\Delta\psi_{m\text{-}c}$), 3) in middle electrolyte adjacent to the AEM ($\Delta\psi_{m\text{-}a}$), and 4) in positive electrolyte adjacent to the AEM ($\Delta\psi_{p\text{-}a}$). As such, $\Delta\Psi_N = \Delta\psi_{n\text{-}c} + \Delta\psi_{m\text{-}c} + \Delta\psi_{p\text{-}a} + \Delta\psi_{m\text{-}a}$.

There are two Donnan potential differences built in the double-membrane cell: 1) across CEM between negative electrolyte and middle electrolyte ($\Delta\psi_{CEM}$); and 2) across AEM between middle electrolyte and positive electrolyte ($\Delta\psi_{AEM}$). Then, $\Delta\Psi_D = \Delta\psi_{CEM} + \Delta\psi_{AEM}$.

The detailed calculation of each component is described in the following part. The calculation was performed in MATLAB and the corresponding code is attached.

(1) Calculation of the potential difference through Nernst boundary layer

Eq. 2 below shows the dependence of the voltage loss across the middle electrolyte channel on the concentration polarization at each membrane (first term on right hand side) and the resistivity of the middle channel electrolyte (ρ_x). The concentration polarization term is adapted from a boundary layer analysis performed by Braff et. al.[4,5]. The fluid flow is in the positive y-direction with current passing perpendicular to fluid flow.

$$\Delta\psi_{middle} = -2\frac{RT}{z_e F}\ln\left(1 - \frac{i(\tilde{y})}{i_{\lim}(\tilde{y})}\right) + \rho_x d \cdot j(\tilde{y}) \quad \text{Eq. 2}$$

where $\Delta\psi_{\text{middle}}$ stands for voltage loss across the middle electrolyte channel; $\tilde{y} = y/w$, w is the height of middle electrolyte; ρ_x is the resistivity of the middle channel electrolyte; d is the thickness of the middle electrolyte; R is the ideal gas constant; T is temperature; z_e is the charge of the ionic species; F is Faraday's constant; i is current density; i_{lim} is limiting current density given for Poiseuille flow in the middle electrolyte.

$$i_{\text{lim}}(\tilde{y}) = \sqrt[3]{\left(\frac{18\text{Pe}}{\tilde{y}\beta}\right)}\frac{C_{NaCl} z_e D_{NaCl} F}{d \cdot \Gamma(1/3)} \qquad \text{Eq. 3}$$

where D_{NaCl} is the effective diffusion coefficient of sodium chloride: $D_{NaCl} = \frac{2D_{Na^+}D_{Cl^-}}{D_{Na^+} + D_{Cl^-}}$; $\beta = w/d$; w and d are the width and thickness of middle electrolyte, respectively; $\text{Pe} = v \cdot w / D_{\text{NaCl}}$; v is the mean velocity of the parabolic velocity profile; C_{NaCl} is the bulk NaCl concentration;

Eq. 2 was solved along $\tilde{y}$ in MATLAB by discretizing in the y direction. The mesh was refined until the solution was insensitive to the mesh size (n=100). $i(\tilde{y})$ was first solved such that the total potential drop was constant for all $\tilde{y}$ and the total current matched experiments. Next, the concentration polarization term through Nernst boundary layer was tabulated (at each y position) to find its contribution to the total potential drop at various middle channel conditions, based on Eq. 4.

$$\Delta\psi_N(\tilde{y}) = -2\frac{RT}{z_e F}\ln\left(1 - \frac{i(\tilde{y})}{i_{\text{lim}}(\tilde{y})}\right) \qquad \text{Eq. 4}$$

The concentration polarization term through the Nernst boundary layer was then integrated along $\tilde{y}$ to obtain $\Delta\Psi_{\text{N}}$. The variable `ASRcpN` was used to stand for this Nernst potential difference in terms of area-specific resistance in Matlab code.

(2) Calculation of the Donnan potential differences across ion-exchange membrane

The Donnan potential difference across an ion-exchange membrane from electrolyte α to electrolyte β is described as follow:

$$\Delta\psi_D = -\frac{RT}{z_e F}\ln\left(\frac{C_0^\beta + \Delta C^\beta}{C_0^\alpha - \Delta C^\alpha}\right) - \frac{RT}{z_e F}\ln\left(\frac{C_0^\beta}{C_0^\alpha}\right) \qquad \text{Eq. 5}$$

where $\Delta\psi_D$ stands for each of $\Delta\psi_{CEM}$ and $\Delta\psi_{AEM}$; R is ideal gas constant; T is temperature; z_e is the charge of ionic species; F is faraday constant; C^{α} and $C^{\beta}$are the concentration of selecting ion in the vicinity of ion-exchange membrane in electrolyte α and β, respectively; C_0^{α} and C_0^{β} are concentration at open circuit state in electrolyte α and β, respectively; ΔC^{β} and ΔC^{α} are the concentration change in Nernst boundary layer in electrolyte α and β, respectively.

The second term in the equation is to offset static Donnan potential which does not contribute to the concentration-overpotential here.

The concentration change in Nernst boundary layer can be calculated by

$$\Delta C = \frac{i}{\bar{i}_{\lim}} C_0 \qquad \text{Eq. 6}$$

Where i is the current density, $\bar{i}_{\lim}$ is averaged limiting current density, C_o is the concentration at open circuit state.

Each Donnan potential difference across ion-exchange membrane can be calculated and the variable `ASRcpD` was used to stand for this Donnan potential difference in terms of area-specific resistance in Matlab code.

3.2. Development of cost model.

The RFB cost model is designed for a large scale RFB system (1 MW and 8 WMh). The costs of materials used for calculating costs of redox pairs, and electrolytes, and stacks are listed in supplementary tables. The algorithm to calculate V_{eff}, C_e and C_p is shown as a flow chart in **Fig. S9**.[1,2] The modeling GUI was written in software Qt/C++. The application was compiled with MinGW 4.9.1 for the Windows build and Clang 3.6 for the Mac build; Qt 5.4 libraries were used for both.

(1) Calculation of the unit electrolyte cost (U_e).

The following equation was used to calculate the electrolyte cost, and the results are listed in **Table S1**.

$$U_e = U_r + U_{se} = (u_{r,n} + u_{r,p}) + (u_{se,n} + u_{se,p} + u_{se,m})$$

Where U_e is the electrolyte cost; U_r is the cost of redox pair; U_{se} is the cost of supporting electrolyte (salt/acid/base); $u_{r,n}$ and $u_{r,p}$ are the cost of negative redox pair and the cost of positive redox pair, respectively; $u_{se,n}$, $u_{se,p}$, and $u_{se,m}$ are the cost of

negative supporting base, the cost of positive supporting acid, and the cost of middle supporting salt.

For each electrolyte (negative, positive, and middle), u_r and u_{se} are calculated by the following two equations correspondingly.

$$u_r = P/(n \cdot F \cdot W); \text{ and } u_{se} = P/(n \cdot F \cdot W \cdot \gamma)$$

where P is the chemical price, W is the molecular weight of chemical, and n is the number of working electrons/charges per molecule, F is Faraday's constant, γ is the ratio of the concentration of redox pair to the concentration of corresponding supporting salt/acid/base.

(2) Calculation of the unit stack cost (U_s).

The stack cost was calculated by the following equation, and the results are listed in **Table S2**.

$$U_s = U_{em} + U_m + U_b$$

where U_s is the stack cost, U_{em} is the cost of electrode meterials, U_m is the membrane cost, and U_b is the cost of bipolar plate.

4. Supplementary Tables

Table S1. Electrolyte cost for Zn-Fe RFB and all-V RFB

RFB	U_r (¢/Ah)[a]	U_{ss} (¢/Ah)[b]	U_e (¢/Ah)[c]
Zn-Fe RFB	0.33	0.40	0.73
All-V RFB	7.98	0.10	8.10

[a] The pricing information and detailed calculation are shown in **Table S3**

[b] The pricing information and detailed calculation are shown in **Table S4**

[c] The U_e refers to unit electrolyte cost of full cell. The electrolyte cost at standard cell voltage is calculated as $C_e = U_e/V_{rev}$.

For all-V RFB $C_e = \frac{¢8.1/\text{Ah}}{1.26\ \text{V}} =$ ¢6.4/Wh = \$64/kWh

Table S2. Stack cost for both Zn-Fe RFB and all-V RFB

RFB	U_{em} (\$/m^2)[a]	U_m (\$/m^2)[a]	U_b (\$/m^2)[b]	U_s (\$/m^2)
Zn-Fe RFB	118	345	55	518
All-V RFB	140	500	55	695

[a] Detailed calculation is shown in **Table S5 and Table S6**.

[b] From reference[1].

Table S3 Prices of redox compounds

Compound	Molecular weight (W) (g/mol)	Price (P) (\$/kg)	n	u_r (¢/Ah)
$FeCl_3$	162.5	0.215[a]	1	0.13
ZnO	81.0	1.3[b]	2	0.20
V_2O_5	182.0	11.7[c]	2	3.99

[a] Quoted from Henan Allrich Chemical Co., Ltd.

[b] Quoted from Henan Premtec Enterprise Co.

[c] Quoted from www.metalprices.com

Table S4 Prices of supporting salt/acid/base

Chemical	Molecular weight (W) (g/mol)	Price (P) ($/kg)	n	γ	u_{ss} (¢/Ah)
HCl (33%)	36.5	0.18[a]	1	1	0.074
NaOH	40	0.4[b]	2	0.1	0.30
NaCl	58.5	0.05[c]	1	0.33	0.03
H_2SO_4	98	0.075[d]	2	0.3	0.05

[a] Quoted from A.I.K International Exports
[b] Quoted from Henan Fengbai Commercial Co., Ltd.
[c] Quoted from Weifang Dabang Chemical Industry Co., Ltd.)
[d] From the reference[3]

Table S5. Prices of electrode materials

Electrode materials	Price
Carbon felt, 3.1mm thickness ($ m^{-2})	70[a]
Copper mesh, 0.5 mm thickness and 30×30 grid per square inch ($ m^{-2})	48[b]

[a] From reference [3]
[b] Quoted from TWP, Inc.

Table S6. Prices of membrane materials

Membranes	Price
Nafion 212 cation-exchange membrane ($ m^{-2})	225[a]
Nafion 117 cation-exchange membrane ($ m^{-2})	500[b]
FAA3 anion-exchange membrane, 50 μm thickness ($ m^{-2})	120[c]

[a] From reference [6]
[b] From reference [3]
[c] Quoted from Fuma-Tech, GmbH.

Table S7. Prices of other materials/handling

Materials and handling	Price[a]
Heat Exchanger ($ kW^{-1})	84

Valves ($ per unit)	150
Pipes ($ m^{-1})	8
Bolts ($ per unit)	15
Gaskets ($ per unit)	2.5
Collector plates ($ per unit)	150
Aluminum end plates ($ per unit)	193
6″ PVC ball valve ($ per unit)	285
1″ PVC ball valve ($ per unit)	8.6
PVC pipe 1″ ($ ft^{-1})	0.87
PVC pipe 6″ ($ ft^{-1})	12.49
PVC frame ($ m^{-2})	16.56
Power conditioning system ($ kW^{-1})	210
Labor for electrolyte preparation ($ kWh^{-1})	1
Tank ($ gal^{-1})	0.41
Tank freight ($ $gal^{-1}mile^{-1}$)	0.00011

[a] All prices are from reference [3]

References

1 Shah, A., Tangirala, R., Singh, R., Wills, R. & Walsh, F. A dynamic unit cell model for the all-vanadium flow battery. *J Electrochem Soc* **158**, A671-A677 (2011).

2 Stephenson, D. *et al.* Electrochemical Model of the Fe/V Redox Flow Battery. *J Electrochem Soc* **159**, A1993-A2000 (2012).

3 Viswanathan, V. *et al.* Cost and performance model for redox flow batteries. *J Power Sources* **247**, 1040-1051, doi:DOI 10.1016/j.jpowsour.2012.12.023 (2014).

4 Braff, W. A., Bazant, M. Z. & Buie, C. R. Membrane-less hydrogen bromine flow battery. *Nat Commun* **4**, doi:Artn 2346

Doi 10.1038/Ncomms3346 (2013).

5 Braff, W. A., Buie, C. R. & Bazant, M. Z. Boundary Layer Analysis of Membraneless Electrochemical Cells. *J Electrochem Soc* **160**, A2056-A2063, doi:Doi 10.1149/2.052311jes (2013).

6 Vanadium redox flow batteries, an in-depth analysis. (Electric power research institute, 2007).